



Extreme levels of Canadian wildfire smoke in the stratosphere over central Europe – Part 1: AERONET, MODIS and lidar observations

Albert Ansmann¹, Holger Baars¹, Alexandra Chudnovsky², Moritz Haarig¹, Igor Veselovskii³, Ina Mattis⁴, Patric Seifert¹, Ronny Engelmann¹, and Ulla Wandinger¹

¹Leibniz Institute for Tropospheric Research, Leipzig, Germany

²Tel Aviv University, Department of Geography and Human Environment, Tel Aviv, Israel

³Physics Instrumentation Center of General Physics Institute, Moscow, Russia

⁴Observatory Hohenpeissenberg, German Weather Service, Hohenpeissenberg, Germany

Correspondence to: A. Ansmann
(albert@tropos.de)

Abstract. Light extinction coefficients of 500 Mm^{-1} , about 20 times higher than after the Pinatubo volcanic eruptions in 1991, were observed with lidar in the stratosphere over Leipzig, Germany, on 22 August 2017. A pronounced smoke layer extended from 14–16 km height and was 3–4 km above the local tropopause. Optically dense layers of Canadian wildfire smoke reached central Europe 10 days after injection into the lower stratosphere caused by rather strong pyrocumulonimbus activity over western Canada. The smoke-related aerosol optical thickness (AOT) was close to 1.0 at 532 nm over Leipzig during the noon hours. We present detailed observations of this record-breaking smoke event in a series of two articles. In part 1, we provide an overview of Aerosol Robotic Network (AERONET) sun photometer observations and Moderate Resolution Imaging Spectroradiometer (MODIS) retrievals of AOT and show lidar measurements documenting the aerosol layering and the very high particle extinction coefficients. In part 2 (Haarig et al., 2018), observations with three polarization/Raman lidars are presented, performed at Leipzig after sunset on 22 August to elucidate the optical and microphysical properties of the aged smoke. As shown in this part 1, smoke particles were found throughout the free troposphere (532 nm AOT of 0.3). A pronounced 2-km thick stratospheric smoke layer occurred from 14–16 km height (AOT of 0.6). AERONET and lidar observations indicate peak mass concentrations of $70\text{--}100 \mu\text{g m}^{-3}$ in the stratosphere around noon and a well-defined (accumulation mode) smoke particle size distribution characterized by a large effective radius of 0.3–0.4 μm and the absence of a particle coarse mode.

15 1 Introduction

Exceptionally dense Canadian wildfire smoke layers causing an aerosol optical thickness (AOT) close to 1.0 at 532 nm crossed central Europe (Leipzig, Germany) between 3 and 16 km height on 22 August 2017. Stratospheric particle extinction coefficients at 532 nm reached 500 Mm^{-1} at 15–16 km height, about 3–4 km above the local tropopause, and were thus 20 times higher than the maximum extinction values observed in the stratosphere over central Europe in the winters of 1991 and 1992 after the strong Mt. Pinatubo eruption in June 1991 (Ansmann et al., 1993, 1997; Jäger, 2005). Record-breaking intensive fires combined with the formation of exceptionally strong and well organized pyrocumulonimbus clusters in western



Canada (<https://visibleearth.nasa.gov/view.php?id=90759>, <https://earthdata.nasa.gov/fire-and-smoke-in-canada>) were responsible for these unprecedentedly optically thick stratospheric smoke layers. Fromm et al. (2000, 2003) and Rosenfeld et al. (2007) showed that occasionally significant amounts of fire smoke can reach the stratosphere up to several kilometers (2–3 km) above the local tropopause via the formation of pyrocumulonimbus cloud complexes (Fromm et al., 2010; Peterson et al., 5 2017). As suggested by Rosenfeld et al. (2007), the large amount of particles serving as cloud condensation nuclei (CCN) favors the nucleation of a large number of extremely small liquid water droplets, subsequently the suppression of heterogeneous ice formation in the violent updrafts, the formation of comparably small ice crystals by homogeneous freezing, which at the end leads to a strong suppression of the development of precipitation. The stratospheric cloud anvils dissolve in the extreme dry environment above the tropopause and leave the smoke load behind. Similar scenarios of the aerosol impact on deep convection 10 are described by Andreae et al. (2004); Koren et al. (2010a, b); Connolly et al. (2013), and Grabowski and Morisson (2015).

The 2017 wildfire season (April–September) was the worst ever burning season in British Columbia since recording began in 1950 (<https://globalnews.ca/news/3675434/2017-officially-b-c-s-worst-ever-wildfire-season/>) and exceeds even the year 1958 (855000 ha area burned) with about 900000 ha of burned forest. Figure 1 shows the distribution of fire clusters all over Canada in August 2017 obtained from MODIS (Moderate Resolution Imaging Spectroradiometer) observations. The number of fire 15 pixels with fire radiative power $frp > 50$ MW (for $1\text{ km} \times 1\text{ km}$ pixels) was of the order of 10000 in August 2017. Recent studies suggest a direct link between increasing fire activity in northwestern United States and Canada and changing climate and weather conditions (Liu et al., 2009, 2014; Kitzberger et al., 2017). The summer half year of 2017 was unusually dry in western Canada and helped to create a hot, dry environment with a large reservoir of underbrush which is favorable burning material.

After entering the stratosphere the fire aerosol traveled eastward, crossed Europe, northern Asia, and circled around the globe within less than 20 days (Khaykin et al., 2018). Smoke layers were observed all over Europe with ground-based lidar systems of the European Aerosol Research Lidar Network (EARLINET) (Pappalardo et al., 2014) and further lidars operated in a long-term mode (Khaykin et al., 2018). Stratospheric smoke layers and traces were visible over Europe up to the end of 2017 (Baars et al., 2018b). We never observed such a strong and long lasting stratospheric smoke event with lidars before over 25 Leipzig. On average more than 25% out of all regular EARLINET lidar observations at Leipzig during the summer seasons from 1997–2006 showed North America aerosol signatures in the free troposphere, typically in the height range from 3–8 km, and sometimes even up to the tropopause (Mattis et al., 2003, 2008). However, in only very few cases, enhanced particle extinction coefficients were found above the tropopause with values of $10\text{--}20\text{ Mm}^{-1}$ causing a very low $AOT < 0.02$.

Such a strong smoke event with significant spread of carbonaceous aerosol over large parts of the northern hemispheric 30 stratosphere as in August 2017 has implications for the climate directly by absorbing and scattering of radiation, mainly by black carbon (soot) and to a minor part by brown carbon (organic aerosol component) (see, e.g., Stone et al., 2008; Forrister et al., 2015; Jo et al., 2016; Zhang et al., 2017), and indirectly by influencing the evolution and life cycle of ice clouds in the upper troposphere. The direct effect is especially strong over snow and ice-covered surfaces, i.e., over polar regions and leads to a warming of the atmosphere. The indirect effect may be long lasting as in the case of volcanic aerosols, but will be 35 different from the impact of volcanic particles which are mostly liquid sulfuric acid droplets and thus influence ice particle



nucleation and cirrus life cycle via homogeneous freezing (Jensen and Toon, 1992; Sassen et al., 1995; Liu and Penner, 2002). The smoke (soot) particles are solid and thus can serve as ice-nucleating particles in heterogeneous (deposition) freezing processes (Hoose and Möhler, 2012). The stratospheric smoke particles with similar sizes as the volcanic particles may enter the upper troposphere from above by slow gravitational settling lasting over months or even years. During every fire season, the stratospheric smoke aerosol particle reservoir may be filled with new particles again. The strength of injection is expected to increase during the upcoming decades as a response to changing climate conditions. Thus modeling of the complex influence of smoke on the global radiation field, chemical processes, and cloud and rain formation (hydrological cycle) will probably become more and more important. High quality and trustworthy modeling is however only possible in close connection with observations as presented here. It is especially necessary to monitor fire smoke events in terms of injection heights, smoke burden, microphysical and optical properties, and smoke decay and removal behavior. Our article is a contribution to this effort.

The consideration of smoke aerosols in atmospheric models is however complicated. As will be shown in a follow-up article (Baars et al., 2018a), many of the stratospheric smoke layers were found to ascend with time. This was already noticed by Khaykin et al. (2018). During August 2017 the layers were about 2–4 km above the tropopause, weeks to months later they were mostly observed above 20 km or even above 25 km, and thus more than 10 km above the tropopause. Upward movements of soot containing layers can be the result of heating of the environmental air masses by solar absorption by the soot particles (de Laat et al., 2012). However, smoke AOTs considerably higher than 1.0 are required to force the warmed, soot-containing air masses to rise. Renard et al. (2008) pointed out that soot particles can also reach the middle stratosphere owing to the gravito-photophoresis effect (Rohatschek, 1996; Pueschel et al., 2000; Cheremisin et al., 2005). By absorbing solar and terrestrial radiation, coarse soot particles with diameters $D > 1 \mu\text{m}$ can ascend with time without an air-heating (convection) effect, and thus even at rather low $\text{AOT} < 0.05$. Favorable atmospheric conditions for a gravito-photophoresis-related upward motion are given around 20 km height which is in agreement with the existence of a black carbon aerosol layer from 18–21 km as reported by Strawa et al. (1999). Renard et al. (2008) found from balloon-borne and satellite observations that soot particles, originating from biomass burning around the globe, contribute to the aerosol population in the height range from 22–30 km at all latitudes. This height range is clearly above the altitudes directly reached by fire plumes in cases of strong pyrocumulonimbus activity. The ascend and descend behavior of the smoke layers and changes in the optical and microphysical properties of the aged smoke during the second half of 2017 will be illuminated in two further papers which are in preparation (Baars et al., 2018a, b).

Here, we present the observations taken on 22 August 2017 in two articles. In part 1, we discuss Aerosol Robotic Network (AERONET) sun photometer AOT observations at Leipzig and Lindenberg (about 180 km to the northeast of Leipzig), satellite AOT retrievals (MODIS), and lidar observation of aerosol layering and extinction coefficients with focus on the smoke conditions observed during the noon hours of 22 August, when the thickest smoke layers crossed Leipzig. In part 2 (Haarig et al., 2018), we highlight our unique triple-wavelength polarization/Raman lidar observations. For the first time, particle extinction coefficients, depolarization ratios, and extinction-to-backscatter ratios (lidar ratios) were measured at all three important lidar



wavelengths of 355, 532 and 1064 nm in aged tropospheric and stratospheric smoke layers. Very different smoke optical and microphysical properties were found in the troposphere and stratosphere.

2 Instrumentation

2.1 Polly lidar

5 On 22 August 2017 a five-channel single-wavelength 532 nm Polly (*Portable lidar system*) (Althausen et al., 2009; Engelmann et al., 2016; Baars et al., 2016) was run at the Leipzig EARLINET lidar station (51.3°N, 12.4°W, 125 m above sea level) and provided continuous time series of aerosol profiles throughout the day. In addition, a triple-wavelength Polly of the Leibniz Institute for Tropospheric Research (TROPOS) was continuously measuring at Kosetice (49.6°N, 15.1°E, 500 m above sea level), Czech Republic. This lidar was involved in a three-month field campaign. Kosetice is located 275 km southeast of Leipzig. During
10 the smoke event northwesterly winds prevailed in the stratosphere and the air masses crossed Leipzig about four hours before reaching Kosetice.

The so-called Fernald method (Fernald, 1984) was used to derive height profiles of particle extinction coefficient from the lidar observations at daytime. The reference height was set around 10–11 km height (tropopause region) on 22 August and as input lidar ratio we used a value of 70 sr for 532 nm. This lidar ratio of 70 sr was measured with our Raman lidars after sunset
15 on 22 August 2017 (see part 2). To reduce the influence of signal noise the signal profiles have to be smoothed. We used vertical gliding-averaging window length of 185 m in the boundary layer (up to 2.5 km height) and 750 m (above the boundary layer up to 16 km height). The sensitivity tests with different smoothing lengths of 175 m, 350 m, and 750 m in the free troposphere revealed that the main layering features are well resolved by using the comparably large vertical window length of 750 m. The large smoothing length was necessary because the densest smoke layers crossed the lidar at Leipzig during the noon hours
20 when the signal noise by sunlight was highest.

Temperature and pressure profiles are required in the lidar data analysis to correct for Rayleigh extinction and backscattering. This information is taken from the GDAS (Global Data Assimilation System) data base which contains profiles of temperature and pressure from the National Weather Service's National Centers for Environmental Prediction (NCEP) (GDAS, 2018) with a horizontal resolution of 1°. We ignore a minor ozone absorption effect at 532 and 607 nm in the determination of smoke
25 extinction coefficient. The neglect is of the order of a few percent.

In Sect. 3, we will also show height-time displays of the volume depolarization ratio. This quantity is defined as the ratio of cross-to-co-polarized backscatter coefficient. Co and cross denote the planes of polarization (for which the receiver channels are sensitive) parallel and orthogonal to the plane of linear polarization of the transmitted laser pulses, respectively. The volume depolarization ratio enables us to identify non-spherical particles such as ice crystals and irregularly shaped smoke particles.
30 The volume depolarization ratio is comparably high when the particles are non-spherical in shape and very low (almost zero) if the particles are spherical such as soot particles with a liquid shell.



2.2 AERONET sun/skyphotometer

The EARLINET station at Leipzig is collocated with an Aerosol Robotic Network site (Holben et al., 1998). The AERONET sun/sky photometer is operated since 2001 and measures AOT at eight wavelengths from 339 to 1638 nm (AERONET, 2018). Sky radiance observations at four wavelengths complete the AERONET observations. From the spectral AOT distribution for the wavelength range from 440 to 870 nm the wavelength dependence of AOT expressed in terms of the Ångström exponent AE is obtained. Furthermore, the fine mode fraction FMF (fraction of fine-mode AOT to total AOT), and particle size distribution for the entire vertical column can be derived (O'Neill et al., 2003). Fine mode particles have per definition a diameter of $\leq 1 \mu\text{m}$. The full set of AOT and sky radiance measurements are used to derive the particle size distribution (Dubovik et al., 2006).

We further included AERONET observations at Lindenberg, Germany, about 180 km northeast of Leipzig in our studies. The size distribution of the smoke particles could be derived from the Leipzig AERONET observations in the early morning of 22 August and at Lindenberg in the early morning hours of 23 August 2017.

2.3 MODIS

MODIS aboard the NASA Terra and Aqua satellites have been in operation since 2000 and 2002, respectively, providing retrieval products of aerosol and cloud properties with nearly daily global coverage (Remer et al., 2013). The MODIS dark target algorithms over land (with spatial resolution of 10 km and 3 km) perform a simultaneous inversion of the measured top of the atmosphere reflectance in three channels (centered at wavelengths of 466, 645, and 2113 nm) to retrieve total spectral AOT, fine model weighting parameter, and surface reflectance at 2113 nm (Remer et al., 2013) from the MODIS data. The most recently released MODIS Collection 6 product MOD04_3K (for Terra) and MYD04_3K (for Aqua) contains AOT at a 3 km horizontal resolution in addition to the L2 10 km product (Remer et al., 2013; Levy et al., 2015). The retrieval algorithm of the higher resolution product is similar to that of the 10 km standard product with several exceptions (for more details, see http://modis-atmos.gsfc.nasa.gov/MOD04_L2). Validation against surface sun photometer shows that two-thirds of the 3 km retrievals fall within the expected error on a regional comparison but with a high bias of 0.06 especially over urban surfaces. The uncertainty in the retrieved AOT is $0.05 \pm 0.15 \times \text{AOT}$ for $\text{AOT} \leq 1.0$ (Levy et al., 2010, 2013). In our study (Sect. 3), we used the MODIS Collection 6 (C006) AOT retrievals at $3 \text{ km} \times 3 \text{ km}$ (at nadir) spatial resolution collected with Terra (10:30 local equatorial crossing time) and Aqua (13:30 local equatorial crossing time) over Leipzig on 22 August 2017 (MODIS, 2018). We show AOT for 500 nm.

3 Observations

Figure 2 shows four photographs taken in the evening of 22 August 2017, about 250 km northwest and thus upstream of Leipzig. Unusually long filament-like structures over the entire horizon could be observed by eye. Cirrus features are very different and much more heterogeneous. Similar indications for the presence of a massive stratospheric aerosol layer and a coherent large-scale aerosol transport in the stratosphere were observable in the first winter after the Mt. Pinatubo eruption,



when volcanic aerosol layers occurred from the tropopause up to 25–30 km height with 500 nm AOTs of about 0.25. The smoke layer in the stratosphere was estimated to be at 15–16 km height on 22 August from the occurrence of a strong purple light about 20–25 minutes after sunset. Purple light is a mixture of Rayleigh scattered sunlight (predominantly blue light) and red sunlight (remaining after attenuation by Rayleigh extinction) scattered by smoke particles.

5 Figure 3 provides an overview of aerosol layering over central Europe from 20–23 August 2017. We used the Kosetice observations because this lidar was continuously running on these days, while the Polly at Leipzig was sporadically operated only, e.g., not continuously on 21 and 23 August 2017. As can be seen, large coherent smoke structures were observed in the troposphere as well as in the stratosphere over more than one day. Cirrus clouds developed in the smoky environment on 20 and 21 August 2017. Unfortunately, boundary layer clouds (below about 2–3 km height) disturbed aerosol and cloud profiling
10 considerably during the daytime periods. The tropopause height was mainly between 10 and 11.5 km from 20–23 August. The wind velocity decreased with height from the tropopause to 16 km height (GDAS, 2018) which may explain the apparent upward motion of the stratospheric layer. Wind shear may have tilted the smoke plume so that the base of the extended smoke field was detected with lidar first and the upper part of the plume about one day later. The volume depolarization ratio is highest in the cirrus clouds (containing strongly light-depolarizing hexagonal ice crystals) and is also significantly enhanced in the
15 stratospheric smoke layer (caused by irregularly shaped smoke particles). The tropospheric smoke-related volume depolarization ratios were comparably small, indicating the dominance of spherical (compact) particles. The different light-depolarizing features of the tropospheric and stratospheric smoke particles will be discussed in detail in part 2 (Haarig et al., 2018).

The HYSPLIT backward trajectories (Stein et al., 2015; Rolph et al., 2017; HYSPLIT, 2018) in Fig. 4 provide an impression of the air flow during the last 10 days (12–21 August 2017) for heights in the middle and upper troposphere. Strong convective
20 processes as required to lift smoke up to the upper troposphere and lower stratosphere can not be resolved by global circulation models. So, the HYSPLIT trajectories should be interpreted with caution when pyrocumulonimbus activities come into play and influence the vertical smoke exchange and long-range transport. According to the backward trajectories, the smoke traveled about 7–10 days at tropospheric as well as stratospheric height from western Canada to central Europe. This is in good agreement with the travel time derived from the spaceborne lidar observation presented by Khaykin et al. (2018).

25 Figures 5 shows the Leipzig AERONET observations from 21–23 August 2017. Level 1.0 data are presented. In the case of Level 1.5 data, too many valid observations are removed by the automated AERONET cloud screening procedure. We performed a careful cloud screening of the Level 1.0 data by checking the Ångström exponent and the 1640 nm AOT which sensitively varies with the occurrence of cirrus. In this way we avoided that the automated AERONET cloud screening analysis removed, e.g., the observations of the maximum AOT of 1.1 around 11 UTC on 22 August 2017. The respective Ångström
30 exponent was 1.2. The lidar observations (diamonds in Fig. 5) conducted between 11:00–12:00 UTC are in good agreement with the extraordinarily high 500 nm AOT. According to our lidar observations, cirrus clouds were absent during the noon hours of 22 August 2017 so that the shown AERONET smoke observations were not affected by any cloud occurrence.

As can be seen in Fig. 5, FMF increased from values below 0.8 to close to 1 when the smoke layers dominated from noon on 21 August to the evening of 22 August. Accordingly the coarse-particle-related AOT_c was almost zero, and the total AOT was
35 almost equal to the fine-mode AOT_f . This indicates that coarse particles were almost absent. The Ångström exponent (for the



spectral range from 440–870 nm) was mostly between 1.1–1.4 which is indicative for the presence of a pronounced particle accumulation mode.

The AOT values derived from the Polly lidar observations after sunset (20:40–23:00 UTC) are also in good agreement with the AERONET observations. The Leipzig and Lindenberg AERONET stations measured smoke-related AOTs of about 0.4 just before sunset (Leipzig) and after sunrise on the next morning at 6:00 UTC (Lindenberg, not shown). The two lidar AOT values for the 11:00–12:00 UTC period were computed by using a low, but not unrealistic smoke lidar ratio of 50 sr in the lidar retrieval and the lidar ratio of 70 sr as measured with our Raman lidars after sunset on 22 August 2017 (see part 2).

The boundary-layer 500 nm AOT was around 0.1–0.15 on 21 and 23 August 2017 (before and after the smoke period) and about 0.15–0.2 on 22 August as the lidar observations at Leipzig and Kosetice indicated. Thus, the fire smoke layers caused a 532 nm AOT close to 1.0 during the noon hours of 22 August 2017.

Satellite (MODIS) observations of AOT corroborate the lidar and sun photometer measurements. The cloud fields in Fig. 6a provide an impression of the cumulus cloud distribution in the morning of 22 August 2017 (10:15 local time) which hampered the AERONET observations and the MODIS retrieval efforts. Only a few AOT values for 3 km × 3 km pixels could be retrieved from the MODIS observations. However, these few AOT values in Figs. 6a and 6b clearly point to AOT values of the order of 1.0 at 500 nm in the Leipzig area, north and south of the Leipzig AERONET station. Northwesterly winds prevailed on this day in the free troposphere and lower stratosphere.

Figure 7 shows the lidar profiles for the 11:00–12:00 UTC period and the nighttime hours. At noon, the entire free troposphere showed traces of smoke aerosol. The 532 nm AOT was 0.3 in the free troposphere (from about 2.5 km height up to the tropopause) and 0.6 in the stratosphere for the height range from the tropopause up to 16 km height. The smoke-related AOT was significantly lower in the evening hours (blue curve) with a free tropospheric contribution of 0.08 and a stratospheric contribution of 0.2–0.25.

The high stratospheric AOT of 0.6 over Leipzig is in good agreement with CALIOP measurements (Khaykin et al., 2018). The maximum stratospheric smoke AOT measured with CALIOP was of the order of 1.0 at 532 nm. These values occurred over northeastern Canada on 17–19 August 2017 and thus a few days upstream of central Europe. Khaykin et al. (2018) reported maximum AOTs of 0.7, but these values were directly estimated from the height profiles of the attenuated backscatter coefficients and were not corrected for particle extinction influences. If we take smoke extinction (according to an AOT of the order of 0.7–1.0) into account, the true profile of the particle backscatter coefficient multiplied by a smoke lidar ratio of 70 sr leads to an AOT about a factor of 1.5 higher than the apparent one given by Khaykin et al. (2018) and thus to values of the order of 1.0.

Figure 8 shows AERONET and lidar inversion products. The AERONET size distributions were downloaded from the AERONET data base (AERONET, 2018). Details to the lidar data inversion are given in part 2 (Haarig et al., 2018). According to the AERONET size distributions, the smoke-dominated aerosol column showed a pronounced accumulation mode centered at a radius of 200–300 nm at the beginning of the smoke period (Leipzig, 22 August, 5:48 UTC) and at 300–400 nm at the end of the smoke event (Lindenberg, 23 August, 5:42 UTC). The size distribution was clearly shifted to larger sizes compared to the fine mode caused by central European anthropogenic pollution as observed over Lindenberg during smoke-free conditions



in the afternoon of 23 August 2017 (blue curve in Fig. 8). The effective radius r_{eff} of the particles was comparably large with values of 0.33–0.42 μm and the fine-mode-related effective radii $r_{\text{eff},f}$ of 0.23–0.32 μm . Coarse mode particles were almost absent. The remaining weak impact of coarse particles on the volume size distribution for the entire vertical column is probably related to the occurrence of soil and road dust in the boundary layer. The smoke layers vanished in the morning of 23 August.

5 The 500 nm AOT rapidly decreased over Lindenberg from 0.4 (at 6 UTC) to about 0.1 (at 8 UTC). In the late afternoon of 23 August, anthropogenic haze dominated. The dense smoke layers had left Germany. The effective radius decreased to typical values for anthropogenic pollution ($r_{\text{eff}}=0.24 \mu\text{m}$, $r_{\text{eff},f}=0.14 \mu\text{m}$).

The lidar-derived size distribution (from the nighttime measurements) fits very well into the AERONET observations at Lindenberg in the early morning of 23 August. The effective radius r_{eff} of the smoke particles in the stratospheric layer was
10 0.32 μm and thus very close to the Lindenberg values. To obtain a column-integrated quantity that can be comparable with the AERONET observations we multiplied the size-resolved volume concentrations by a vertical extent of the stratospheric layer of 1000 m (see Fig. 7). This volume size distribution for the stratospheric smoke layer (column) is shown as black curve in Fig. 8.

Further lidar inversion products are given in Fig. 8 for the evening smoke conditions. Because the peak values of the particle
15 extinction coefficient at 532 nm was a factor of 2 higher during the noon hours, peak mass concentrations were in the range of 70–100 $\mu\text{g m}^{-3}$ in the stratosphere around noon of 22 August 2017. The retrieved single scatter albedo (see part 2 for more explanations concerning the retrieval) of 0.8 at 532 nm clearly indicates strongly light-absorbing smoke (soot) particles in the stratosphere.

Similar size distributions with a pronounced smoke accumulation mode shifted to larger sizes were found during several
20 airborne in situ measurements of North American wildfire plumes in the European region (Fiebig et al., 2002; Petzold et al., 2007; Dahlkötter et al., 2014). All these airborne in situ observations indicated that super micrometer particles (coarse-mode particles) were almost absent in the aged smoke plumes and that the accumulation mode was enhanced and shifted towards larger mode diameters.

After the illumination of the optical and size-distribution aspects, Fig. 9 finally deals with the shape properties of the strato-
25 spheric smoke particles. As will be explained in detail in part 2 a surprisingly strong wavelength dependence of the particle linear depolarization ratio was observed with lidar in the stratosphere. As mentioned above, the particle linear depolarization ratio is rather sensitive to changes in shape properties. The depolarization ratio is almost zero for spherical particles and significantly enhanced for non-spherical, irregularly shaped particles. On 22 August 2017, the stratospheric smoke depolarization ratio was highest with 22% at 355 nm and lowest with 4% at 1064 nm, about a factor of 4–5 lower. We hypothesize that this
30 strong wavelength dependence is the consequence of a missing particle coarse mode. As shown in Fig. 9, a similar wavelength dependence is also observable in the case of non-spherical desert dust particles in the absence of a dominating coarse mode (Järvinen et al., 2016; Mamouri and Ansmann, 2017). Especially, the 355 nm and 532 nm particle depolarization ratios for stratospheric smoke and fine-mode dust particles are rather similar.



4 Conclusions

Extreme levels of Canadian fire smoke were observed in the stratosphere on 22 August 2017. Extinction coefficients reached values of 500 Mm^{-1} and were thus about a factor of 20 higher than maximum extinction values found over central Europe after the Pinatubo eruption. Such high stratospheric extinction coefficients were never observed over Leipzig before and are related to the record-breaking fire season in western Canada in 2017. A pronounced stratospheric smoke layer extended from 14–16 km height and was about 3–4 km above the local tropopause. We analyzed AERONET, MODIS and lidar observations to document this record-breaking stratospheric smoke event. Maximum smoke-related AOTs were close to 1.0 and the stratospheric particle mass concentrations reached $70\text{--}100 \mu\text{g m}^{-3}$. The smoke particles formed a well-defined aged accumulation mode characterized by a large effective radius of $0.3\text{--}0.4 \mu\text{m}$.

This extreme case presented here demonstrates that significant amounts of wildfire smoke can reach the stratosphere and can significantly disturb the stratospheric aerosol conditions (Khaykin et al., 2018) and may thus have a sensitive influence on chemical processes, radiative fluxes, and even heterogeneous ice formation in the upper troposphere and this over months after each summer fire season. The black carbon aerosol partly enriches the natural soot particle reservoir between 20–30 km by upward motions, probably caused by gravito-photophoresis forces (Renard et al., 2008).

We will continue and deepening the characterization of the smoke optical and microphysical properties in the troposphere and stratosphere in part 2 (Haarig et al., 2018). Very different smoke optical and microphysical properties were found in the troposphere and stratosphere. Based on the results of part 1 and part 2, an extended conclusion section is given in part 2.

5 Data availability

The Polly lidar data are available at TROPOS upon request (info@tropos.de). Backward trajectories analysis has been supported by air mass transport computation with the NOAA (National Oceanic and Atmospheric Administration) HYSPLIT (Hybrid Single-Particle Lagrangian Integrated Trajectory) model (HYSPLIT, 2018) using GDAS meteorological data (Stein et al., 2015; Rolph et al., 2017). AERONET sun photometer AOT data are downloaded from the AERONET web page (AERONET, 2018). We used the ftp site for MODIS data download: https://ladsweb.modaps.eosdis.nasa.gov/allData/6/MOD04_3K/ (MODIS, 2018).

Acknowledgements. The authors gratefully acknowledge the NOAA Air Resources Laboratory (ARL) for the provision of the HYSPLIT transport and dispersion model. We are also grateful to AERONET for providing high quality sun photometer observations, calibrations, and products. Special thanks to the Lindenberg AERONET team to carefully run the station. This activity is supported by ACTRIS Research Infrastructure (EU H2020-R&I) under grant agreement no. 654109. The development of the lidar inversion algorithm was supported by the Russian Science Foundation (project 16-17-10241).



References

- AERONET: AERONET aerosol data base, available at: <http://aeronet.gsfc.nasa.gov/>, last access: 20 February, 2018.
- Althausen, D., Engelmann, R., Baars, H., Heese, B., Ansmann, A., Müller, D., and Komppula, M.: Portable Raman Lidar PollyXT for Automated Profiling of Aerosol Backscatter, Extinction, and Depolarization, *J. Atmos. Oceanic Tech.*, 26, 2366–2378, doi:10.1175/2009JTECHA1304.1, 2009.
- 5 Andreae, M. O., Rosenfeld, D., Artaxo, P., Costa, A. A., Frank, G. P., Longo, K. M., and Silva-Dias, M. A. F.: Smoking rain clouds over the Amazon, *Science*, 303, 1337–1342, doi:10.1126/science.1092779, 2004.
- Ansmann, A., Wandinger, U., and Weitkamp, C.: One-year observations of Mount-Pinatubo aerosol with an advanced Raman lidar over Germany at 53.5°N, *Geophys. Res. Lett.*, 20, 711–714, doi: 10.1029/93GL00266, 1993.
- 10 Ansmann, A., Mattis, I., Wandinger, U., Wagner, F., Reichardt, J., and Deshler, T.: Evolution of the Pinatubo Aerosol: Raman Lidar Observations of Particle Optical Depth, Effective Radius, Mass, and Surface Area over Central Europe at 53.48°N, *J. Atmos. Sci.*, 54, 2630–2641, [https://doi.org/10.1175/1520-0469\(1997\)054<2630:EOTPAR>2.0.CO;2](https://doi.org/10.1175/1520-0469(1997)054<2630:EOTPAR>2.0.CO;2), 1997.
- Baars, H., Kanitz, T., Engelmann, R., Althausen, D., Heese, B., Komppula, M., Preißler, J., Tesche, M., Ansmann, A., Wandinger, U., Lim, J.-H., Ahn, J. Y., Stachlewska, I. S., Amiridis, V., Marinou, E., Seifert, P., Hofer, J., Skupin, A., Schneider, F., Bohlmann, S., Foth, A., Bley, S., Pfüller, A., Giannakaki, E., Lihavainen, H., Viisanen, Y., Hooda, R. K., Pereira, S. N., Bortoli, D., Wagner, F., Mattis, I., Janicka, L., Markowicz, K. M., Achtert, P., Artaxo, P., Pauliquevis, T., Souza, R. A. F., Sharma, V. P., van Zyl, P. G., Beukes, J. P., Sun, J., Rohwer, E. G., Deng, R., Mamouri, R.-E., and Zamorano, F.: An overview of the first decade of PollyNET: an emerging network of automated Raman-polarization lidars for continuous aerosol profiling, *Atmos. Chem. Phys.*, 16, 5111–5137, doi:10.5194/acp-16-5111-2016, 2016.
- Baars et al., Upward transport of stratospheric smoke from Canadian forest fires, to be submitted to ACP, as contribution to the EARLINET special issue, 2018a.
- 20 Baars et al., Tropospheric and stratospheric smoke over Europe as observed within EARLINET/ACTRIS in the summer of 2017, to be submitted to ACP, as contribution to the EARLINET special issue, 2018b.
- Burton, S. P., Hair, J. W., Kahnert, M., Ferrare, R. A., Hostetler, C. A., Cook, A. L., Harper, D. B., Berkoff, T. A., Seaman, S. T., Collins, J. E., Fenn, M. A., and Rogers, R. R.: Observations of the spectral dependence of linear particle depolarization ratio of aerosols using NASA Langley airborne High Spectral Resolution Lidar, *Atmos. Chem. Phys.*, 15, 13453–13473, doi:10.5194/acp-15-13453-2015, 2015.
- 25 Cheremisin, A. A., Vassilyev, Yu. V., and Horvath, H.: Gravitational photophoresis and aerosol stratification in the atmosphere, *J. Aerosol. Sci.*, 36, 1277–1299, doi:10.1016/j.jaerosci.2005.02.003, 2005.
- Connolly, P. J., Vaughan, G., May, P. T., Chemel, C., Allen, G., Choularton, T. W., Gallagher, M. W., Bower, K. N., Crosier, J. and Dearden, C.: Can aerosols influence deep tropical convection? Aerosol indirect effects in the Hector island thunderstorm. *Q.J.R. Meteorol. Soc.*, 139: 2190–2208. doi:10.1002/qj.2083, 2013.
- 30 Dahlkötter, F., Gysel, M., Sauer, D., Minikin, A., Baumann, R., Seifert, P., Ansmann, A., Fromm, M., Voigt, C., and Weinzierl, B.: The Pagami Creek smoke plume after long-range transport to the upper troposphere over Europe – aerosol properties and black carbon mixing state, *Atmos. Chem. Phys.*, 14, 6111–6137, <https://doi.org/10.5194/acp-14-6111-2014>, 2014.
- de Laat, A. T. J., Stein Zweers, D. C., Boers, R., and Tuinder, O. N. E.: A solar escalator: Observational evidence of the self-lifting of smoke and aerosols by absorption of solar radiation in the February 2009 Australian Black Saturday plume, *J. Geophys. Res.*, 117, D04204, doi:10.1029/2011JD017016, 2012.
- 35



- Dubovik, O., Sinyuk, A., Lapyonok, T., Holben, B., Mishchenko, M., Yang, P., Eck, T., Volten, H., Muñoz, O., Veihelmann, B., van der Zande, W. J., Leon, J. F., Sorokin, M., and Slutsker, I.: Application of spheroid models to account for aerosol particle non-sphericity in remote sensing of desert dust, *J. Geophys. Res.*, 111, D11208, doi:10.1029/2005JD006619, 2006.
- Engelmann, R., Kanitz, T., Baars, H., Heese, B., Althausen, D., Skupin, A., Wandinger, U., Komppula, M., Stachlewska, I. S., Amiridis, V., Marinou, E., Mattis, I., Linné, H., and Ansmann, A.: The automated multiwavelength Raman polarization and water-vapor lidar PollyXT: the neXT generation, *Atmos. Meas. Tech.*, 9, 1767–1784, doi:10.5194/amt-9-1767-2016, 2016.
- Fernald, F. G.: Analysis of atmospheric lidar observations: some comments, *Appl. Opt.*, 23, 652–653, doi.org/10.1364/AO.23.000652, 1984.
- Fiebig, M., Petzold, A., Wandinger, U., Wendisch, M., Kiemle, C., Stifter, A., Ebert, M., Rother, T., and Leiterer, U.: Optical closure for an aerosol column: Method, accuracy, and inferable properties applied to a biomass-burning aerosol and its radiative forcing, *J. Geophys. Res.*, 107, 8130, doi:10.1029/2000JD000192, 2002.
- Forrister, H., Liu, J., Scheuer, E., Dibb, J., Ziemba, L., Thornhill, K. L., Anderson, B., Diskin, G., Perring, A. E., Schwarz, J. P., Campuzano-Jost, P., Day, D. A., Palm, B. B., Jimenez, J. L., Nenes, A., and Weber, R. J., Evolution of brown carbon in wildfire plumes. *Geophys. Res. Lett.*, 42, 4623–4630. doi: 10.1002/2015GL063897, 2015.
- Freeborn, P. H., Wooster, M. J., Roy, D. P., Cochrane, M. A.: Quantification of MODIS fire radiative power (FRP) measurement uncertainty for use in satellite-based active fire characterization and biomass burning estimation, *Geophys. Res. Lett.*, 41, 1988–1994, doi: 10.1002/2013GL059086, 2014.
- Fromm, M., Alfred, J., Hoppel, K., Hornstein, J., Bevilacqua, R., Shettle, E., Servranckx, R., Li, Z., Stocks, B.: Observations of boreal forest fire smoke in the stratosphere by POAM III, SAGE II, and lidar in 1998, *Geophys. Res. Lett.*, 27, 1407–1410, 2000.
- Fromm, M. D., and Servranckx, R.: Transport of forest fire smoke above the tropopause by supercell convection, *Geophys. Res. Lett.*, 30, 1542, doi:10.1029/2002GL016820, 2003.
- Fromm, M., Shettle, E. P., Fricke, K. H., Ritter, C., Trickl, T., Giehl, H., Gerding, M., Barnes, J., O'Neill, M., Massie, S. T., Blum, U., McDermid, I. S., Leblanc, T., and Deshler, T.: The stratospheric impact of the Chisholm Pyrocumulonimbus eruption: 2. Vertical profile perspective, *J. Geophys. Res.*, 113, D08203, doi:10.1029/2007JD009147, 2008.
- Fromm, M., Lindsey, D. T., Servranckx, R., Yue, G., Trickl, T., Sica, R., Doucet, P., and Godin-Beekmann, S. E.: The untold story of pyrocumulonimbus, *B. Am. Meteorol. Soc.*, 91, 1193–1209, doi:10.1175/2010bams3004.1, 2010.
- GDAS: Global Data Assimilation System, meteorological data base, available at: <https://www.ready.noaa.gov/gdas1.php>, last access: 20 February, 2018.
- Grabowski, W. W., and Morrison, H.: Untangling microphysical impacts on deep convection applying a novel modeling methodology. Part II: double-moment microphysics, *J. Atmos. Sci.*, 73, 3749–3770, <https://doi.org/10.1175/JAS-D-15-0367.1>, 2016.
- Haarig, M., Ansmann, A., Althausen, D., Klepel, A., Groß, S., Freudenthaler, V., Toledano, C., Mamouri, R.-E., Farrell, D. A., Prescod, D. A., Marinou, E., Burton, S. P., Gasteiger, J., Engelmann, R., and Baars, H.: Triple-wavelength depolarization-ratio profiling of Saharan dust over Barbados during SALTRACE in 2013 and 2014, *Atmos. Chem. Phys.*, 17, 10767–10794, <https://doi.org/10.5194/acp-17-10767-2017>, 2017.
- Haarig, M., Ansmann, A., Baars, H., Jimenez, C., Veselovskii, I., Engelmann, R., and Althausen, D.: Extreme levels of Canadian wildfire smoke in the stratosphere over central Europe – Part 2: Lidar study of depolarization and lidar ratios at 355, 532, and 1064 nm, and microphysical properties, *ACP*, submitted, 2018.



- Holben, B. N., Eck, T. F., Slutsker, I., Tanré, D., Buis, J. P., Setzer, A., Vermote, E., Reagan, J. A., Kaufman, Y. J., Nakajima, T., Lavenu, F., Jankowiak, I., and Smirnov, A.: AERONET – a federated instrument network and data archive for aerosol characterization, *Remote Sens. Environ.*, 66, 1–16, 1998.
- Hoose, C. and Möhler, O.: Heterogeneous ice nucleation on atmospheric aerosols: a review of results from laboratory experiments, *Atmos. Chem. Phys.*, 12, 9817–9854, <https://doi.org/10.5194/acp-12-9817-2012>, 2012.
- Hu, Q., Bravo Aranda, J.-A., Popovici, I., Goloub, P., Povdin, T., Veselovskii, I., and Pitras, C.: Observations and analysis of UTLS aerosols detected over North France, *J. Geophys. Res.*, in revision, 2018.
- HYSPLIT: HYbrid Single-Particle Lagrangian Integrated Trajectory model, backward trajectory calculation tool, available at: http://ready.arl.noaa.gov/HYSPLIT_traj.php, last access: 20 February, 2018.
- Jäger, H.: Long-term record of lidar observations of the stratospheric aerosol layer at Garmisch-Partenkirchen, *J. Geophys. Res.*, 110, D08106, doi:10.1029/2004JD005506, 2005.
- Järvinen, E., Kempainen, O., Nousiainen, Kociok, T., Möhler, O., Leisner, T., and Schnaiter, M.: Laboratory investigations of mineral dust near-backscattering depolarization ratios, *J. Quant. Spect. Radiat. Transfer*, 178, 192–208, doi:10.1016/j.jqsrt.2016.02.003.
- Jensen, E. J., and Toon, O. B.: The potential effects of volcanic aerosols on cirrus cloud microphysics, *Geophys. Res. Lett.*, 19, 1759–1762, <http://dx.doi.org/10.1029/92GL01936>, 1992.
- Jo, D. S., Park, R. J., Lee, S., Kim, S.-W., and Zhang, X.: A global simulation of brown carbon: implications for photochemistry and direct radiative effect, *Atmos. Chem. Phys.*, 16, 3413–3432, <https://doi.org/10.5194/acp-16-3413-2016>, 2016.
- Khaykin, S. M., Godin-Beekmann, S., Hauchecorne, A., Pelon, J., Ravetta, F., and Keckut, P.: Stratospheric smoke with unprecedentedly high backscatter observed by lidars above southern France, *Geophys. Res. Lett.*, 45, <https://doi.org/10.1002/2017GL076763>, 2018.
- Kitzberger, T., Falk, D. A., Swetnam, T. W., and Westerling, L.: Heterogeneous responses of wildfire annual area burned to climate change across western and boreal North America, *PLOS One*, 12, e0188486. doi:<https://doi.org/10.1371/journal.pone.0188486>, 2017.
- Koren, I., Remer, L. A., Altaratz, O., Martins, J. V., and Davidi, A.: Aerosol-induced changes of convective cloud anvils produce strong climate warming, *Atmos. Chem. Phys.*, 10, 5001–5010, <https://doi.org/10.5194/acp-10-5001-2010>, 2010a.
- Koren, I., Feingold, G., and Remer, L. A.: The invigoration of deep convective clouds over the Atlantic: aerosol effect, meteorology or retrieval artifact?, *Atmos. Chem. Phys.*, 10, 8855–8872, <https://doi.org/10.5194/acp-10-8855-2010>, 2010b.
- Levy, R. C., Remer, L. A., Kleidman, R. G., Mattoo, S., Ichoku, C., Kahn, R., and Eck, T. F.: Global evaluation of the Collection 5 MODIS dark-target aerosol products over land, *Atmos. Chem. Phys.*, 10, 10399–10420, doi:10.5194/acp-10-10399-2010, 2010.
- Levy, R. C., Mattoo, S., Munchak, L. A., Remer, L. A., Sayer, A. M., Patadia, F., and Hsu, N. C.: The Collection 6 MODIS aerosol products over land and ocean, *Atmos. Meas. Tech.*, 6, 2989–3034, doi:10.5194/amt-6-2989-2013, 2013.
- Levy, R., Hsu, C., et al.: MODIS Atmosphere L2 Aerosol Product. NASA MODIS Adaptive Processing System, Goddard Space Flight Center, USA: http://dx.doi.org/10.5067/MODIS/MOD04_L2.006, 2015.
- Liu, X., and Penner, J. E.: Effect of Mount Pinatubo H₂SO₄/H₂O aerosol on ice nucleation in the upper troposphere using a global chemistry and transport model, *J. Geophys. Res.*, 107(D12), doi:10.1029/2001JD000455, 2002.
- Liu, Y., Stanturf, J.A., and Goodrick, S.L.: Trends in global wildfire potential in a changing climate, *For. Ecol. Manage.*, 259, 685–697, doi:10.1016/j.foreco.2009.09.002, 2009.
- Liu, Y., Goodrick, S., and Heilman, W.: Wildland fire emissions, carbon, and climate: Wildfire-climate interactions, *For. Ecol. Manage.*, 317, 80–96, <http://dx.doi.org/10.1016/j.foreco.2013.02.020>, 2014.



- Mamouri, R.-E. and Ansmann, A.: Potential of polarization/Raman lidar to separate fine dust, coarse dust, maritime, and anthropogenic aerosol profiles, *Atmos. Meas. Tech.*, 10, 3403–3427, <https://doi.org/10.5194/amt-10-3403-2017>, 2017.
- Mattis, I., Ansmann, A., Wandinger, U., and Müller, D.: Unexpectedly high aerosol load in the free troposphere over Central Europe in spring/summer 2003, *Geophys. Res. Lett.*, 30, 2178, doi:10.1029/2003GL018442, 2003.
- 5 Mattis, I., Müller, D., Ansmann, A., Wandinger, U., Preißler, J., Seifert, P., and Tesche, M.: Ten years of multiwavelength Raman lidar observations of free-tropospheric aerosol layers over central Europe: Geometrical properties and annual cycle, *J. Geophys. Res.*, 113, D20202, doi:10.1029/2007JD009636, 2008.
- MODIS: MODIS ftp site for data download: https://ladsweb.modaps.eosdis.nasa.gov/allData/6/MOD04_3K/, last access: 19 February, 2018.
- Müller, D., Mattis, I., Wandinger, U., Ansmann, A., Althausen, A., and Stohl, A.: Raman lidar observations of aged Siberian and Canadian forest fire smoke in the free troposphere over Germany in 2003: Microphysical particle characterization, *J. Geophys. Res.*, 110, D17201, doi:10.1029/2004JD005756, 2005.
- 10 O'Neill, N. T., Eck, T. F., Smirnov, A., Holben, B. N., and Thulasiraman, S.: Spectral discrimination of coarse and fine mode optical depth, *J. Geophys. Res.*, 108, 4559, doi:10.1029/2002JD002975, 2003.
- Remer, L.A., Mattoo, S., Levy, R. C., and Munchak, L. A.: MODIS 3 km aerosol product: algorithm and global perspective, *Atmos. Meas. Tech.*, 6, 1829–1844. doi:10.5194/amt-6-1829-2013, 2013.
- 15 Pappalardo, G., Amodeo, A., Apituley, A., Comeron, A., Freudenthaler, V., Linné, H., Ansmann, A., Bösenberg, J., D'Amico, G., Mattis, I., Mona, L., Wandinger, U., Amiridis, V., Alados-Arboledas, L., Nicolae, D., and Wiegner, M.: EARLINET: towards an advanced sustainable European aerosol lidar network, *Atmos. Meas. Tech.*, 7, 2389–2409, doi:10.5194/amt-7-2389-2014, 2014.
- Peterson, D. A., Hyer, E. J., Campbell, J. R., Solbrig, J. E., and Fromm, M. D.: A conceptual model for development of intense pyrocumulonimbus in western North America, *Mon. Wea. Rev.*, 145, 2235–2255, doi.org/10.1175/MWR-D-16-0232.1, 2017.
- 20 Petzold, A., Weinzierl, B., Huntrieser, H., Stohl, A., Real, E., Cozic, J., Fiebig, M., Hendricks, J., Lauer, A., Law, K., Roiger, A., Schlager, H., and Weingartner, E.: Perturbation of the European free troposphere aerosol by North American forest fire plumes during the ICARTT-ITOP experiment in summer 2004, *Atmos. Chem. Phys.*, 7, 5105–5127, doi:10.5194/acp-7-5105-2007, 2007.
- Pueschel, R. F., Verma, S., Rohatschek, H., Ferry, G. V., Boiadjieva, N., Howard, S. D., and Strawa, A. W.: Vertical transport of anthropogenic soot aerosol into the middle atmosphere, *J. Geophys. Res.*, 105(D3), 3727–3736, doi:10.1029/1999JD900505, 2000.
- 25 Reid, J. S., and Hobbs, P. V.: Physical and optical properties of young smoke from individual biomass fires in Brazil, *J. Geophys. Res.*, 103, 32013–32030, doi:10.1029/98JD00159, 1998.
- Renard, J.-B., Brogniez, C., Berthet, G., Bourgeois, Q., Gaubicher, B., Chartier, M., Balois, J.-Y., Verwaerde, C., Auriol, F., Francois, P., Daugeron, D., and Engrand, C.: Vertical distribution of the different types of aerosols in the stratosphere: Detection of solid particles and analysis of their spatial variability, *J. Geophys. Res.*, 113, D21303, doi:10.1029/2008JD010150, 2008.
- 30 Rohatschek, H.: Levitation of stratospheric and mesospheric aerosols by gravito-photophoresis, *J. Aerosol. Sci.*, 27, 467–475, 1996.
- Rolph, G., Stein, A., and Stunder, B.: Real-time Environmental Applications and Display sYstem: READY. *Environmental Modelling & Software*, 95, 210–228, <https://doi.org/10.1016/j.envsoft.2017.06.025>, 2017.
- Rosenfeld, D., Fromm, M., Trentmann, J., Luderer, G., Andreae, M. O., and Servranckx, R.: The Chisholm firestorm: observed microstructure, precipitation and lightning activity of a pyro-cumulonimbus, *Atmos. Chem. Phys.*, 7, 645–659, <https://doi.org/10.5194/acp-7-645-2007>, 2007.



- Sassen, K., Starr, D. O. C., Mace, G. G., Poellot, M. R., Melfi, S. H., Eberhard, W. L., Spinhirne, J. D., Eloranta, E. W., Hagen, D. E., and Hallett, J.: The 5-6 December 1991 FIRE IFO II jet stream cirrus case study: Possible influences of volcanic aerosols, *J. Atmos. Sci.*, 52, 97-123, 1995.
- Schroeder, W., Csiszar, I., Giglio, L., Schmidt, C. C.: On the use of fire radiative power, area, and temperature estimates to characterize biomass burning via moderate to coarse spatial resolution remote sensing data in the Brazilian Amazon, *J. Geophys. Res.-Atmospheres*, 115, D21121, doi:10.1029/2009JD013769, 2010.
- 5 Stone, R. S., Anderson, G. P., Shettle, E. P., Andrews, E., Loukachine, K., Dutton, E. G., Schaaf, C., and Roman III, M. O.: Radiative impact of boreal smoke in the Arctic: Observed and modeled, *J. Geophys. Res.*, 113, D14S16, doi:10.1029/2007JD009657, 2008.
- Strawa, A. W., Drdla, K., Ferry, G. V., Verma, S., Pueschel, R. F., Yasuda, M., Salawitch, R. J., Gao, R. S., Howard, S. D., Bui, P. T., Loewenstein, M., Elkins, J. W., Perkins, K. K., and Cohen, R.: Carbonaceous aerosol (soot) measured in the lower stratosphere during POLARIS and its role in stratospheric photochemistry, *J. Geophys. Res.*, 104, 26753–26766, doi:10.1029/1999JD900453, 1999.
- 10 Stein, A.F., Draxler, R.R., Rolph, G.D., Stunder, B.J.B., Cohen, M.D., and Ngan, F.: NOAA's HYSPLIT atmospheric transport and dispersion modeling system, *Bull. Amer. Meteor. Soc.*, 96, 2059-2077, <http://dx.doi.org/10.1175/BAMS-D-14-00110.1>, 2015
- Wandinger, U., Müller, D., Böckmann, C., Althausen, D., Matthias, V., Bösenberg, J., Weiß, V., Fiebig, M., Wendisch, M., Stohl, A., and Ansmann, A.: Optical and microphysical characterization of biomass-burning and industrial-pollution aerosols from multiwavelength lidar and aircraft measurements, *J. Geophys. Res.*, 107(D21), doi:10.1029/2000JD000202, 2002.
- 15 Zhang, Y., Forrister, H., Liu, J., Dibb, J., Anderson, B., Schwarz, J.P., Perring, A. E., Jimenez, J. L., Campuzano-Jost, P., Wang, Y., Nenes, A., and Weber, R. J.: Top-of-atmosphere radiative forcing affected by brown carbon in the upper troposphere, *Nature Geoscience*, 10, 486-489, doi:10.1038/ngeo2960, 2017.

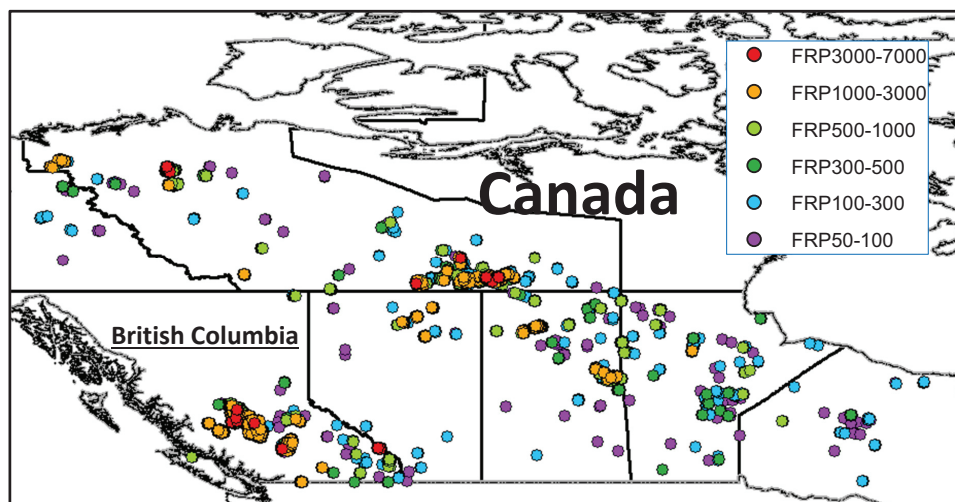


Figure 1. Fires detected with MODIS aboard the Terra and Aqua satellites over Canada in the period from 1-31 August 2017. The six color-coded classes of FRP (fire radiative power in MW for 1 km×1 km pixels) indicate different fire strengths (intensity of biomass burning) (Schroeder et al., 2010; Freeborn et al., 2014). The MODIS (MCD14DL) product is downloaded (<https://earthdata.nasa.gov/earth-observation-data/near-real-time/firms/active-fire-data>).



Figure 2. Stratospheric aerosol layer photographed near Hannover (Steinhuder Sea), Germany, about 250 km northwest (or 3–4 hours upwind) of Leipzig. The photos (top left, top right, bottom left) are taken around sunset at 18:33 UTC and at 18:40 UTC (bottom right). At 18:55 UTC (22 minutes after sunset) strong purple light was visible caused by the layer at 15–16 km height. Long filament-like structures covered the sky.

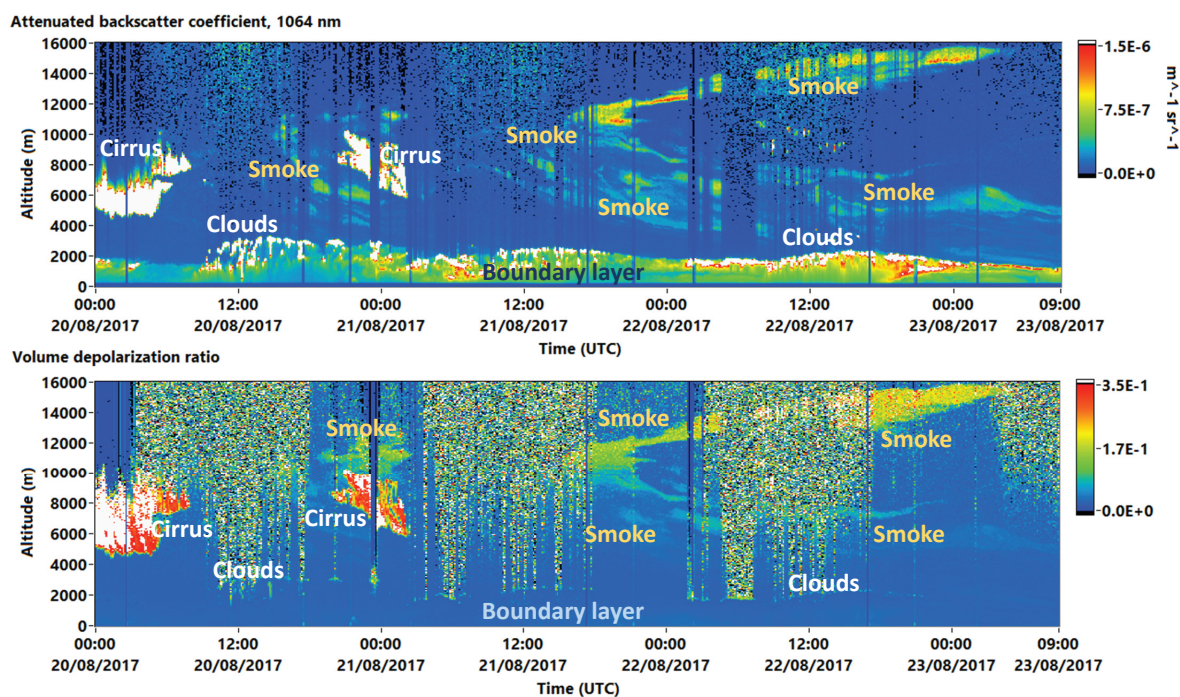


Figure 3. Canadian wildfire smoke layers in the troposphere and stratosphere over Kosetice, Czech Republic, observed with lidar on 20–23 August 2017. The uncalibrated attenuated backscatter coefficient (range-corrected signal) at 1064 nm (top) and the volume depolarization ratio at 532 nm (bottom) are shown. The tropopause was at 10–11.5 km height (20 August), 10.5–12 km height (21 August), and 10.5–11.5 km height (22 August).

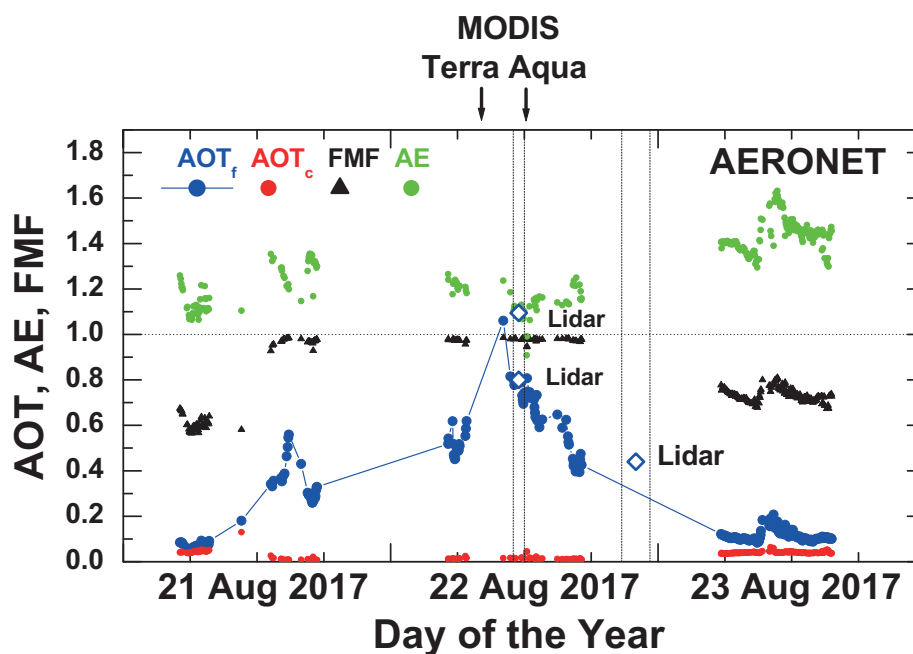


Figure 5. AERONET sun photometer observations at Leipzig (TROPOS) from 21–23 August 2017. 500 nm fine-mode AOT_f (blue circles) and coarse-mode AOT_c (red circles), Ångström exponents AE (green circles, for the 440–870 nm wavelength range), and fine-mode fraction FMF (black triangles, for 500 nm AOT) are shown. Gaps in the time series are caused by cloud fields and night time hours. Dashed vertical lines indicate the lidar measurement periods around noon and at nighttime (Fig. 7). The lidar-derived 532 nm AOT (diamonds) are given in addition. AOTs of 0.8 and 1.1 are obtained with an input lidar ratio of 50 sr and 70 sr (measured after sunset of this day), respectively. The horizontal line at 1.0 indicates that most FMF values were close to 1.0 during the passage of the smoke layers and that the Ångström exponent was clearly above 1.0 in most case. The overpass times of MODIS Terra and Aqua are indicated above the figure. MODIS results are shown in Fig. 6.

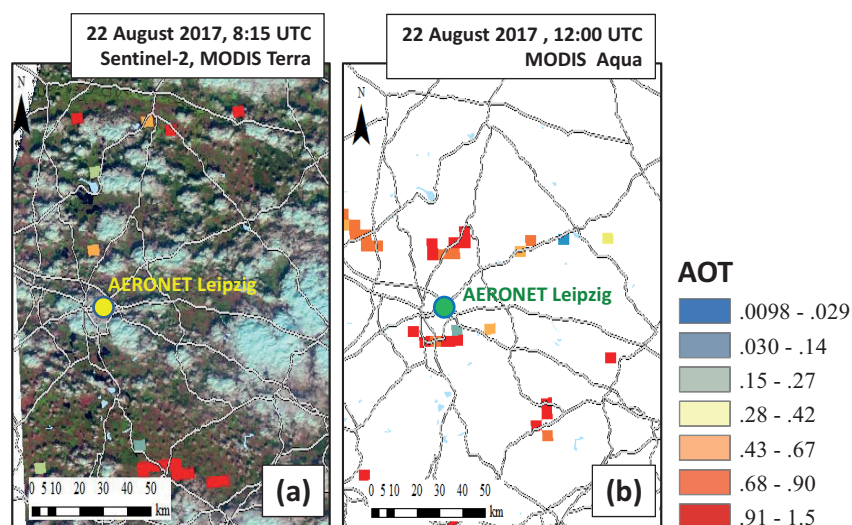


Figure 6. (a) Sentinel-2 cumulus cloud fields (bluish-white) for 8:30 UTC equatorial crossing time (Leipzig, overpass at 8:15 UTC), and integrated MODIS Terra color-scaled 500 nm AOT values for 3 km×3 km cloud-free areas, (b) respective MODIS Aqua 500 nm AOT retrievals for 11:30 UTC equatorial crossing time (Leipzig, overpass at 12:00 UTC). The yellow and green circles indicate the AERONET Leipzig site. Many red squares (AOT of 0.9-1.5) were retrieved from the MODIS observations south and north of the AERONET station.

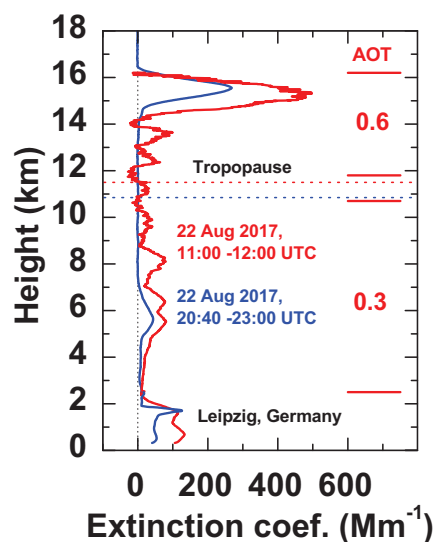


Figure 7. Height profile of particle extinction coefficient at 532 nm over Leipzig on 22 August 2017 measured with Polly close to noon (red profile), when the optically densest stratospheric smoke layers crossed the lidar site, and at nighttime (blue profile). The nighttime observations with three lidars will be discussed in part 2 (Haarig et al., 2018). The Fernald method was applied to compute the extinction profiles. An input lidar ratio of 70 sr (as measured after sunset, see part 2) was used. The AOTs for the free troposphere and lower stratosphere are given as numbers.

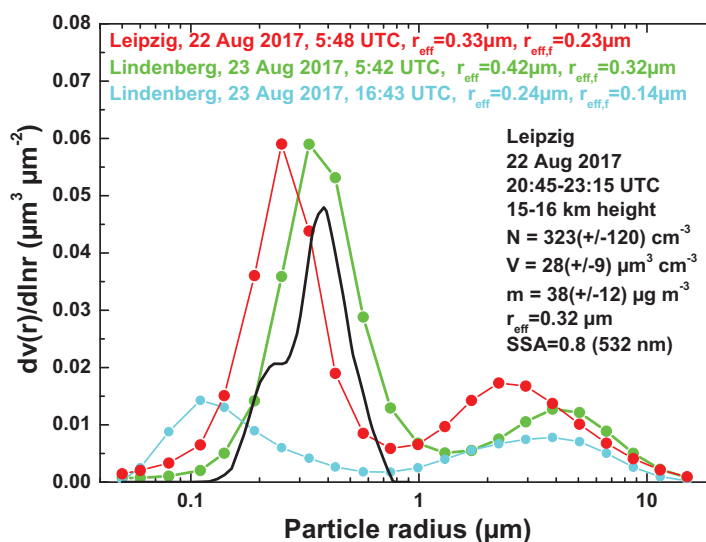


Figure 8. Particle volume size distributions derived from AERONET sun photometer observations at Leipzig (red) and Lindenberg (blue, green). Effective radii (r_{eff} for the total size distribution, $r_{\text{eff},f}$ for the pronounced fine or accumulation mode) indicate that the aged smoke particles were comparably large. Accumulation-mode particles dominated the optical properties. The volume size distribution is considerably shifted towards larger sizes compared to the pure anthropogenic fine mode (in blue). The lidar-derived size distribution (in black) for the stratospheric layer alone agrees well with the AERONET observations and indicates that the pronounced accumulation mode is caused by smoke particles. The retrieval of the size distribution and listed microphysical smoke values for the 15–16 km layer are discussed in the text and in part 2. Mean values of the particle number concentration N , volume concentration V , mass concentration m , effective radius r_{eff} , and single scattering albedo SSA for the stratospheric layer are given as numbers.

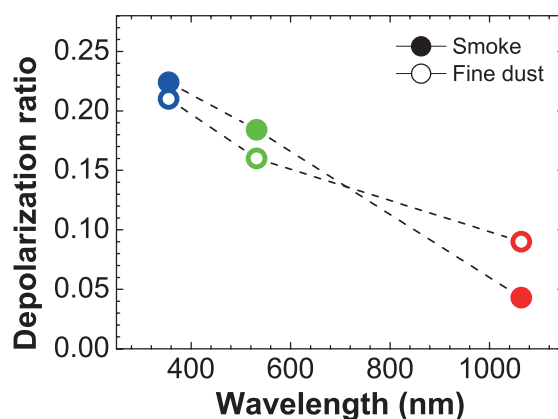


Figure 9. Spectral dependence of particle linear depolarization ratio for fine dust (Mamouri and Ansmann, 2017; Järvinen et al., 2016) and fire smoke (Haarig et al., 2018).